Accelerated White Etch Cracking (WEC) FE8 type tests of different bearing steels using ceramic rollers

Danielsen, H.K.; Gutiérrez Guzmán, F.; Fæster, S.; Shirani, M.; Rasmussen, B.H.; Linzmayer, M.; Jacobs, G.

Published in:
Wear

Link to article, DOI:
10.1016/j.wear.2021.204230

Publication date:
2022

Document Version
Publisher's PDF, also known as Version of record

Wear 494–495 (2022) 204230

Contents lists available at ScienceDirect

Wear

journal homepage: www.elsevier.com/locate/wear

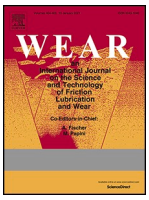

Accelerated White Etch Cracking (WEC) FE8 type tests of different bearing steels using ceramic rollers

H.K. Danielsen [a,*], F. Gutiérrez Guzmán [b], S. Fæster [a], M. Shirani [a], B.H. Rasmussen [a], M. Linzmayer [b], G. Jacobs [b]

[a] Technical University of Denmark, Department of Wind Energy, Frederiksborgvej 399, 4000, Roskilde, Denmark
[b] RWTH Aachen University, Institute for Machine Elements and Systems Engineering (MSE), Schinkelstrasse 10, 52062, Aachen, Germany

A B S T R A C T

White Etch Cracking (WEC) is a severe and unpredictable failure mode affecting bearings in various industrial sectors. In this work, accelerated WEC laboratory tests have been performed using FE8 type test rigs with ceramic rollers to test the WEC resistance of different bearing materials, materials quality and roughness. It is demonstrated that the test method can reliably and consistently provoke WEC in commercially available washers. Tests using washers with different roughness values did not show significant changes in the time to failure. Tests of through hardened bearing steel with a low content of inclusions resulted in a significantly longer time to failure compared to the baseline. Through hardened washers with a black oxide coating did not improve the WEC life as the coating was worn away during testing. Tests with two types of carbo-nitrided washers gave significantly longer time to failure, of which one type in particular showed high resistance towards WEC formation.

1. Introduction

White Etch Cracking (WEC) is a well known cause of premature failures in wind turbine gearbox bearings, resulting in macro-pitting. The issue is not limited to a specific product, manufacturer or country, but must rather be considered as a generic issue pertaining to the whole wind energy sector. WEC is not specific to the wind energy sector, it is present in many other sectors including transport, construction and other industrial sectors [1–4]. WEC consists of subsurface crack networks surrounded by a microstructure of nano-sized ferritic grains with dissolved carbides [5–12] which is substantially harder than the matrix, normally referred to as white etching areas or white etching matter due to the white appearance in light optical microscopy after etching. There are still disagreements on the WEC failure mechanism in the literature and the root causes are still being researched [13–17]. For example, some sources indicate that the hard white nanostructure causes the cracks [18,19] while others indicate crack rubbing causes the hard white nanostructure [20,21]. Some preventive measures have been implemented by bearing, gearbox and wind turbine manufacturers, typically using new bearing types or bearing configurations based on best practice. Several WEC resistant bearing materials based on surface treatments are currently available, including carburization, induction hardening and black oxide coating as well as bearings made from high-end expensive nitrogen rich steels. However, either these solutions do not offer 100 % guarantee against WEC or are significantly more expensive than current standard bearings [22–24].

When observed in the wind energy sector, WEC has a severe failure progression with experienced bearing life often within 20 % of calculated life [2,17,25]. In order to reproduce WEC in workshop tests, certain specific test conditions are needed to be imposed on the specimens. This can include using hydrogen pre-charging of the specimens [26–28], using specific lubricants [29–31], introducing excessive slip [32–34] or external electrical currents [35,36]. One of the most common accelerated WEC tests is the FE8 type test rigs with axial cylindrical roller bearings, which have been extensively used for studying WEC [7,14,15,17,24,29,30,37–42]. It relies on the inherent slip in 81212 type bearings, as well as using WEC inducing lubricants. In line with expectations, it is well known that through hardened steel rolling elements are vulnerable to WEC [41]. Tests of WEC resistant or WEC immune materials relies on testing of washer specimens and refrain from testing rolling element specimens due to manufacturing and cost reasons. Therefore, tests must either include interruptions for changing the through hardened steel rolling elements or use ceramic rollers, which are unaffected by WEC as previously has been demonstrated in Ref. [24].

While most studies deal with examining the root causes of WEC through investigating test parameters, such as lubricant or slip, only few studies have focused on comparing the WEC resistance of different bearing materials. Gould et al. [22] have used a micropitting rig to assess

* Corresponding author.
E-mail address: hkda@dtu.dk (H.K. Danielsen).

https://doi.org/10.1016/j.wear.2021.204230
Received 30 July 2021; Received in revised form 3 December 2021; Accepted 26 December 2021
Available online 28 December 2021

the WEC resistance of carburized AISI 3310 test specimens against standard through hardened AISI 52100 bearing steel. This showed an increased lifetime of around 2.3x of the carburized test specimens compared to the through hardened specimens. Blass et al. [24] have used an FE8 test rig and ceramic rollers to assess the WEC resistance of several types of steels, including SAE 4320 case carburized steel, 50CrMo4mod induction hardened QT steel as well as Cronidur 30 high nitrogen stainless steel. The case carburized specimens showed no improvements over through hardened martensitic or bainitic specimens, whereas the induction hardened specimens had the lifetime increased with a factor of 2. The Cronidur 30 specimens did not fail, even after being tested for 10 times the duration of normal through hardened specimens.

The main purpose of this work is to compare the WEC resistance for different bearing materials using FE8 type accelerated WEC tests. Within the framework of this work ceramic rolling elements are used for conducting uninterrupted tests. Washer test specimens were acquired for different types of through hardened and surface treated steel materials, which were tested and characterized to evaluate the resistance to WEC formation.

2. Experimental

2.1. Test set-up

The tests presented in this work were conducted using cylindrical roller thrust bearings of type 81212 mounted in two laboratory FE8 test rigs. Deviating from the standard FE8 constant load spring system, the load is applied with a piston inside a hydraulic cylinder. The test rigs include electrical servo-drives with stepless adjustable speeds including shifted 2-speed gearbox for 7.5–4500 rpm with automatic test-stop in case of exceeding temperature, vibration or runtime limit. The test rigs are equipped with accelerometers to detect vibrations caused by bearing damages.

Test conditions for all tests are listed in Table 1. All tests were run with ceramic rolling elements to avoid WEC failure in the rollers. The ceramic Si_3N_4 rolling elements have a Youngs modulus 320 GPa and a Poissons ratio of 0.26. The rolling elements were fitted in polyamide 15 rollers snap-fit cages. Tests were carried out under constant load of 60 kN, the resulting maximum normal contact stress using the surface and sub-surface stress model introduced in Ref. [41] are shown in Fig. 1. As previously described, the contacting bodies are assimilated to half-spaces, and their contact surfaces meshed into a 500 × 500 × 100 (x; y; z) elements grid, with each cuboidal element having a dimension of 0.38 μm × 13 μm × 1.9 μm. The bearing washer is defined as an ideal plane while for the roller a measured profile is used. The used profile has been previously used in Ref. [41] and differs insignificantly from the profile of the ceramic rolling elements. The profiles of the two rolling elements are shown in Fig. 2. By using the Youngs modulus and Poissons ratio of Si_3N_4, the maximum surface contact stress increases by around 11% from 1966 N/mm^2 to 2189 N/mm^2. Accordingly, the calculated magnitude of the maximum Tresca stress in the roller-washer contact increases from 1214 MPa to 1355 MPa and corresponding depth decreases from 142 μm to 134 μm respectively. A detailed model description of the stress state in the used cylindrical roller thrust bearings from type 81212 can be found in Ref. [41].

Table 1
Test conditions used for all tests.

Axial load	60 kN
Contact stress	2189 N/mm^2
Speed	500rpm (300rpm first 24h)
Temperature	100 °C
Lubricant	SAE 75W-80 oil
Oil flow	0.2 l/min
Roller type	Ceramic rollers, 11x11mm
Cage type	15-roller polymer snap-fit cages
Test duration	Until failure (vibration) or time-out

The speed was set to 500 rpm, water cooling of the oil lubricant was used to reach this speed, however a 300 rpm run-in speed was still necessary during the first 24 h due to overheating issues. The housing washer temperature was monitored and controlled using heating elements and air cooling. If the temperature limit was exceeded the test rigs automatically lowered the speed until an equilibrium temperature of 100 °C was reached, if the temperature reached 110 °C the test rigs would automatically shut down. Vibration sensors are fitted to the rigs, for all tests a vibration threshold level was set and if surpassed the tests automatically stopped. All test presented in this work were stopped due to exceeding the vibration threshold level, except for one test which was interrupted due to time-out.

All tests were run using a mineral oil in a circulating lubrication system with filters and an oil flow of 0.2 l/min (0.1 l/min for each bearing). This specific oil is a commercially available, fully formulated automotive gearbox SAE 75W-80 oil with a measured kinematic viscosity of 54.2 mm^2/s at 40 °C and 9.31 mm^2/s at 100 °C. An analysis of the elemental composition is shown in Table 2. In comparison to the previously used lubricant in Refs. [7,29–31] the analysis shows a reduced concentration of Mg-Sulfonate (1950 → 6 ppm) and an increased concentration of Ca-Sulfonate (39 → 757 ppm), which is also considered to promote the formation of WEC [19]. In accordance to previously published work [41], the evaluation of the lubrication conditions was carried out by calculating the specific lubrication film thickness λ_{min} defined in equation (1):

$$\lambda_{min} = \frac{h_{min}}{\sqrt{\left(R^2_{a,Washer} + R^2_{a,Roller}\right)}} \quad (1)$$

The isotherm lubrication film thickness h_{min} was calculated according to Ref. [43].

2.2. Washer specimens

Steel washers from two different major bearing manufacturers were acquired from commercially available bearings, and used as a baseline for evaluating the performance of surface engineered washers. The commercially bought washers were martensitic through hardened 100Cr6 (1.3505) grade steel, see Table 3, and will be noted as MTH A and MTH B for the purpose of this work. Some of the commercial MTH A washers were coated with standard commercial black oxide for evaluating its effect on WEC for this test setup. NSK Germany GmbH provided specially made washers for the FE8 testing campaign. These included commercial grade SUJ2 martensitic through hardened steel washers (MTH C) as well as two versions of case carbo-nitrided washers corresponding to the commercial products of Super-TF™ and AWS-TF™, which will be noted as CN A and CN B respectively for the purpose of this work.

The raceway surface roughness for all of the baseline washers had a R_a value of around 0.08 μm while the roughness of the carbo-nitrided washers were around 0.03 μm. The MTH C washers were tested with both R_a value of 0.03 μm and 0.08 μm to evaluate the effect of the raceway surface roughness. The ceramic rolling elements used in all tests had a surface roughness of 0.05 μm. The R_a roughness values are summarized in Table 4 and the resulting film thicknesses at 100 °C are summarized in Table 5.

2.3. Ultrasound

All tested washers were scanned using ultrasound for detecting subsurface cracks. For ultrasonic scans a Pulse-Echo technique was used with a high frequency HFUS 2000 system with a X, Y, Z scanner immersion scanning system in a 1000 × 700 × 500 mm water tank. During

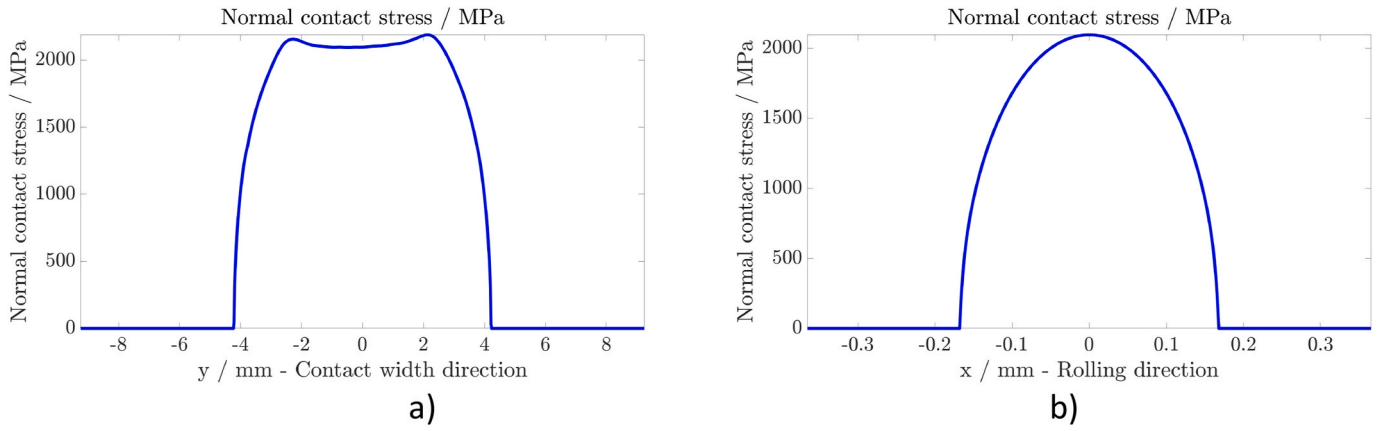

Fig. 1. Pressure distribution (60 kN) in a) width and b) rolling direction.

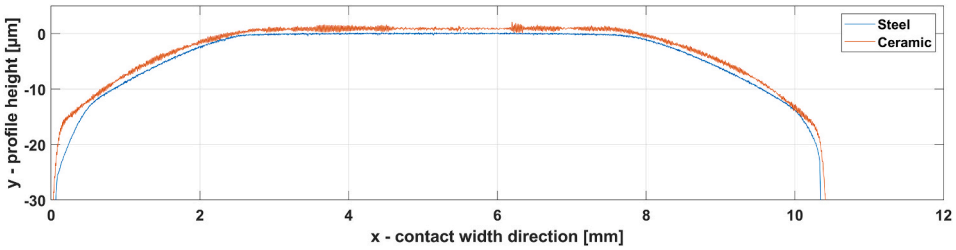

Fig. 2. Plot for the profiles for the ceramic rolling element used in this work and commercial steel rolling element. The x-axis shows the contact width direction (measurement direction) and the y-axis the profile height, the steel profile is shifted upwards by 2 µm to show both profiles in one diagram.

Table 2
Chemical analysis of the used mineral oil measured by inductively coupled plasma atomic emission spectroscopy (ICP).

S	P	Zn	Ca	Mg
2989 ppm	559 ppm	4 ppm	757 ppm	6 ppm

scanning, the peak echo values are measured in two electronic time gates. The first gate is covering the cross section of the bearing and the second gate is covering the back echo from the inner surface of the bearing. Frequency of the transducer is set to 50 MHz and moves in the x- and y-coordinates with a resolution of 0.200 mm (and a −6 dB limit) per measurement in both directions. Scanned objects were cleaned for lubricant oil to avoid aberrations in the scan and dried afterwards to avoid corrosion from the water that acts as medium between the examined object and the transducer.

2.4. Microscopy and hardness measurements

The presence of WEC in the washers was investigated using optical microscopy for which the samples were ground, polished and finally etched with 2% Nital. SEM imaging was done with a TESCAN VEGA3 SBU microscope equipped with an EDAX Element EDS detector. Micro-hardness measurements were conducted on washers using a Vickers hardness measurement tester with a load of 0.2 kg and a dwell time of 20 s. Hardness profiles were made on cross sections from the washer surface down towards the center of the specimens with a step size of 60 µm.

2.5. X-ray tomography

Three samples for X-ray tomography, with the dimensions 1 × 1 × 20 mm, were cut out from the center of tested washers, at which depth the material can be considered to be unaffected by over-rolling. The

Table 4
Roughness of washer and rolling elements used in this work.

Component	Roughness Ra (µm)
Ceramic rolling elements	0.05
MTH A & B washers	0.08
MTH C washers	0.08 & 0.03
CN A & B	0.03

Table 5
Specific film thickness used in this work.

Washers	Speed	Specific film thickness at 100 °C
MTH A, MHT B, MHT C (R_a 0.08)	300 rpm (first 24 h)	0.33
	500 rpm	0.47
CN A, CN B, MTH C (R_a 0.03)	300 rpm (first 24 h)	0.54
	500 rpm	0.77

Table 3
Composition for standard bearing steels.

Designation	Steel grade	Standard	C	Mn	Si	Cr
MTH A & B	100Cr6 (1.3505)	ISO 683-17	0.90–1.05	0.25–0.45	0.15–0.35	1.35–1.65
MTH C	SUJ2	JIS G4805	0.95–1.10	0–0.50	0.15–0.35	1.30–1.60

central part of the samples was scanned by X-ray tomography using a Zeiss Xradia 520 Versa. 5001 projections were acquired using a scan energy of 140 keV and an exposure time of 6 s. The reconstructions were performed by a standard filtered back projection resulting in a reconstructed volume with a voxel size of 0.85 μm. A cube of 847 x 847 x 847 voxels corresponding to 720 × 720 × 720 μm where extracted from the bulk of the sample. The size of the extracted volume was chosen to match the standard ISO 4967 for classifying defects using standard microscopy in bearing steel.

3. Results

3.1. Bearing tests and time to failure analysis

Ten tests using commercially bought washers, MTH A and MTH B, were performed in order to establish a baseline for the chosen test conditions. The tests performed comparably and ran within the 60–100 h range, see Table 6. All tests failed in a similar manner with spalling on the washer raceway, see Fig. 3a, with ultrasound measurements showing presence of extensive subsurface cracks, which was confirmed to be WEC by optical microscopy. The combined average time to failure was 76.9 h. By means of a Weibull analysis [44] the lifetime of the MTH A washers at a failure probability of 10 % (B_{10}) was determined to be 69.8 h. This lifetime correlates to a high degree with previously published results using 100Cr6 steel/steel bearings under similar tribological conditions. In Ref. [45] the experimentally determined lifetime at a failure probability of 10 % (B_{10}) was 70.9 h. It is worth mentioning, that 100Cr6 steel/steel bearings under a similar pressure have a calculated nominal service life at a failure probability of 10 % (L_{10h}) of 394.64 h and a calculated modified service life at a failure probability of 10 % (L_{10mh}) according to DIN ISO 281 [46] of 54.5 h [45]. However, by using oils which do not lead to the formation of WEC the running times are much higher (>500 h) [29]. A comparison of the experimentally determined lifetime at a failure probability of 10 % (B_{10}) with the lifetime L_{10h} or L_{10mh} cannot be conducted in this work due to the unknown bearing dynamic load ratings (C) for non-standard bearings (hybrid bearings or other non-standard materials). A Weibull analysis of the MTH B washers is not possible due to the low sample size. The Weibull line is also characterized by the so-called shape parameter beta (β), with a higher shape parameter indicating a reduced statistical scatter of the test results. In previously conducted WEC investigations under similar load conditions using through hardened steel rollers, a different lubricant and a reduced speed a shape parameter beta (β) in the range 2.8 between 4.7 was identified [41]. As seen in Fig. 4 the beta value for the conducted experiments using MTH A washers is 9.9 and, therefore, in the range of the beta values mentioned in Ref. [42]. It is worth noting that typical values for classical fatigue tests are in the range between 1 and 2 [44,47,48]. The high reproducibility (coefficient of correlation of 0.888) and low scattering (β = 9.9) show the improved suitability of the selected testing methodology for risk assessment of thrust bearings. A detailed description of the conducted Weibull analysis can be found in previous publications of the authors [41,45].

An identical test was performed on MTH A washers that had been coated with black oxide, MTH A BO. The test ran for a similar time as the other baseline tests, with the same type of WEC failure mode confirmed by ultrasound and microscopy. This indicates that the black oxide had no effect on the failure mode or time to failure, and visual inspection showed the black oxide coating was completely worn off in the contact zone with the rollers, see Fig. 3b. Four tests were run using MTH C washers, which had a similar failure mode as the other baseline tests, confirmed as WEC with ultrasound and microscopy investigations, however they had a significantly longer time to failure. The MTH C tests were performed using two different roughness, two test each with R_a = 0.03 μm and R_a = 0.08 μm respectively. The roughness difference did not seem to affect the time to failure substantially as all of the MTH C tests failed within the 300–400 h time interval.

Two tests were run using CN A washers, which had roughly the same time to failure as the MTH C tests. Again, the failure mode was very similar to the baseline tests, with ultrasound measurements indicating extensive subsurface cracks verified to be WEC by optical microscopy. Two tests were run using CN B washers, and although both tests ran substantially longer than the other tests, ultrasound measurements did not show any indication of subsurface cracks in these washers. One of the test ran until time-out, no spalling was observed on the washers. The other test ran more than ten times longer than the baseline tests, but a failure on one of the rollers was observed, see Fig. 5, as well as spalling on the raceway, thus it is unknown what caused the failure.

Table 6
Overview of the accelerated WEC tests and cause of failure. MTH are Martensitic Through Hardened washers and CN are Carbo-Nitrided washers.

Washer material	Time to failure	Shaft Revolutions	Failure location	Sub-surface cracks by ultrasound
MTH A 1	67.5h	1,727,071	Washer	Yes
MTH A 2	71.5h	1,856,268	Washer	Yes
MTH A 3	72.3h	1,863,851	Washer	Yes
MTH A 4	72.6h	1,667,111	Washer	Yes
MTH A 5	75.1h	1,962,557	Washer	Yes
MTH A 6	79.4h	2,094,465	Washer	Yes
MTH A 7	89.5h	2,390,658	Washer	Yes
MTH A 8	97.2h	2,588,654	Washer	Yes
MTH A BO	79.9h	2,107,477	Washer	Yes
MTH B 1	66.9h	1,711,958	Washer	Yes
MTH B 2	76.8h	2,012,795	Washer	Yes
MTH C 1 (R_a 0.03)	305.6h	8,879,077	Washer	Yes
MTH C 2 (R_a 0.03)	332.8h	9,694,987	Washer	Yes
MTH C 3 (R_a 0.08)	379.9h	11,104,077	Washer	Yes
MTH C 4 (R_a 0.08)	388.4h	11,363,013	Washer	Yes
CN A 1	337.6h	9,840,969	Washer	Yes
CN A 2	372.8h	10,736,505	Washer	Yes
CN B 1	898.7h	26,671,687	Washer + roller	No
CN B 2	1411.3h	42,047,869	Timeout	No

3.2. Failure characterization

When tests where finished, visual inspection was performed on all washers. For all tests that stopped due to vibration, spalling was found on the washers, similar to what is shown in Fig. 3. For the CN B test 1, a failed ceramic roller was also observed, in addition to a spall on the washer. The failed ceramic rollers left regular imprints on the washers that matched the contours of the failure in the roller, see Fig. 5. It was impossible to determine if roller or washer failure occurred first.

After visual inspection, all tested washers were scanned for subsurface cracks using ultrasound measurements, which indicated the level of WEC in the washers. An example is shown in Fig. 6, showing all four washers from the two bearings from the MTH A 6 test. The notches at the 12 clock positions of the washers are used for positioning to extract areas of interest for optical microscopy. Location of subsurface cracks can be seen as small green-blueish patches, mainly along the inner and/or outer band of the raceway, corresponding to the locations where negative slip and positive slip respectively take place. The spalled areas can be identified as larger blue areas. For comparison the spalls shown in Fig. 3a are located in Fig. 6b on the right washer (note that the ultrasound images are based on the back echo, and thus are inversed). Most of the tested washers without presence of surface spalls still showed some indication of subsurface cracks in varying intensity, indicating different stages of WEC formation.

Optical microscopy investigations of washers from each material type were investigated to verify the presence of WEC, see examples in Fig. 7. Cross-section samples were extracted from raceways of washers

Fig. 3. Visual inspection of spalling on washers from a) MTH A 6 test (prior to ultrasound scan) and b) the MTH A BO test (after ultrasound scan).

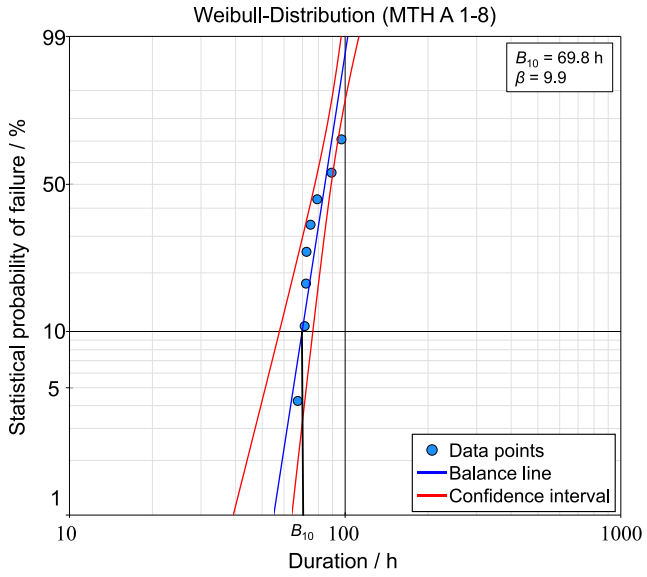

Fig. 4. Weibull distribution from the MTH A tests.

with and without indication of subsurface cracks by ultrasound. The ultrasound measurement technique was an effective method to detect and locate WEC, also discussed in previous work [41]. Cuts preferentially made at sites where ultrasound indicated presence of sub-surface cracks always contained WEC, whereas no cracks could be found for cross sections at sites without subsurface crack indications from ultrasound measurements.

During the investigation of the root cause failure for CN B 1 test (roller and washer failure), a small cluster of WEC was found using optical microscopy directly beneath the spalled area, see Fig. 8. While this demonstrates that WEC can form in the carbo-nitrided CN B material, it is unknown if the found WEC beneath the spall caused the failure of CN B 1 test. Aside from this area, no signs of subsurface cracks were observed for any of the CN B washers using ultrasound measurements, however it is not possible to investigate areas directly beneath the spall with this technique. There is a chance of local WEC having formed in other locations on the washer if the formation was too small for ultrasound detection, although no further WEC was found using optical microscopy at other locations.

3.3. Material characterization

Measurement of the hardness profiles for the carbo-nitrided washers were performed to investigate the depth of the diffusion layers. Although the hardness profiles were dissimilar, the hardened zone was observed to be up to 2 mm deep for both carbo-nitrided versions, see Fig. 9. This depth is more than sufficient to cover the WEC formation zone for FE8 tests. As discussed above, the test conditions used in this work result in a maximum Tresca stress of 1355 MPa at 134 μm. For the martensitic through hardened washers, the hardness were measured as 742, 747 and 786 $HV_{0.2}$ respectively for MTH A, MTH B and MTH C.

Due to the large difference in time to failure between MTH C and MTH A/MTH B, nominally all equivalent steel grades with similar roughness (R_a = 0.08 μm), 3D tomography scans were performed on these washers for comparing the cleanliness of the material, such as inclusion size and distribution. In order to observe smaller inclusions, several steps were taken to filter out the background noise. First the

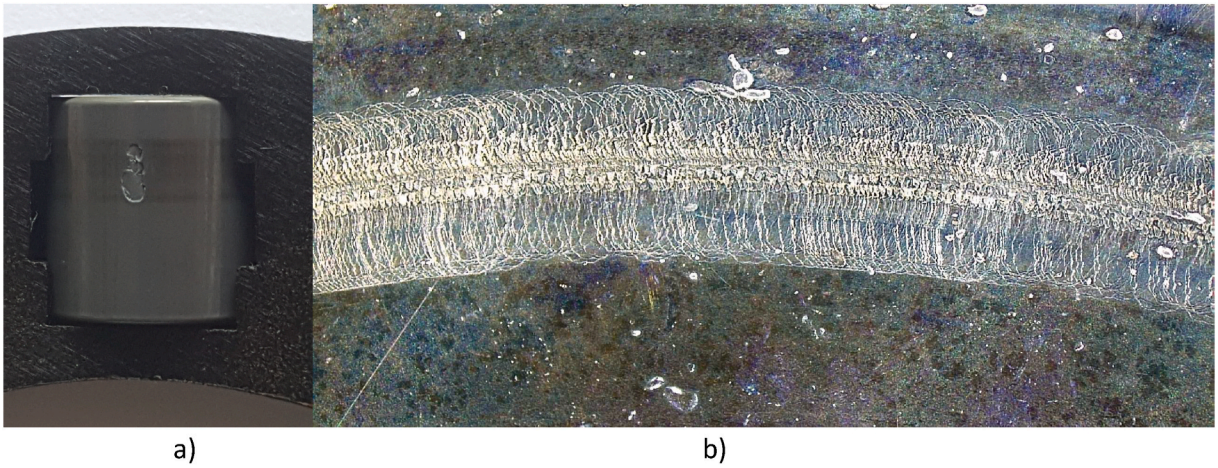

Fig. 5. a) Failed ceramic roller from CN B 1 test and b) imprints from the ceramic roller on the corresponding housing washer (after ultrasound scan).

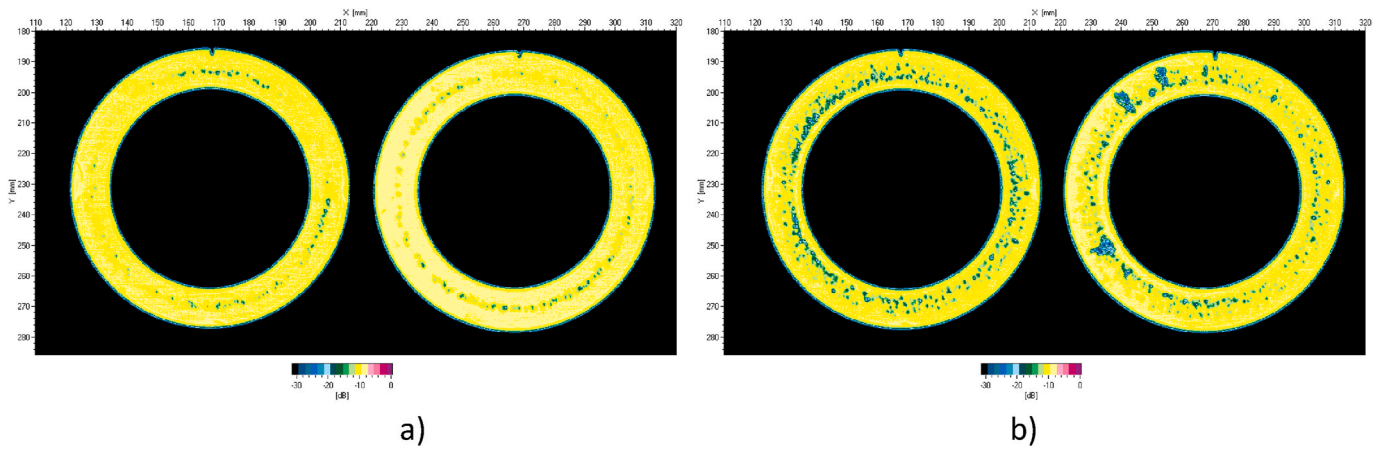

Fig. 6. Ultrasound scans of washers, green-blueish patches indicate subsurface cracks while larger mostly blueish patches indicate spalling on the raceway surface. a) Bearing 1 washers and b) bearing 2 washers from the MTH A 6 test are shown. Shaft washers are located on the left and housing washer on the right (the bearing 2 housing washer is also shown in Fig. 3a). Since the measurements are based on the back echo, all images are inverse. (For interpretation of the references to colour in this figure legend, the reader is referred to the Web version of this article.)

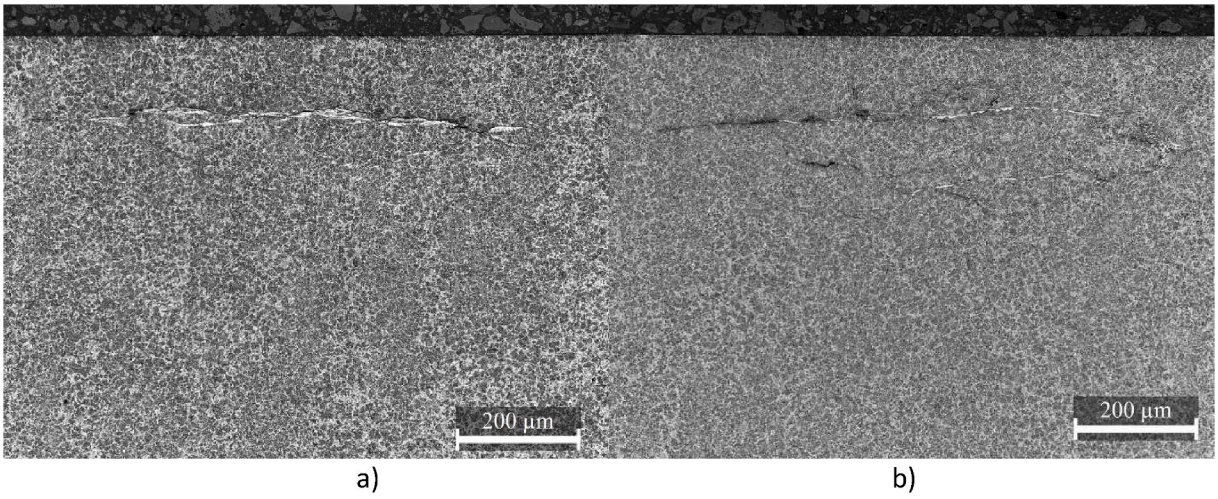

Fig. 7. Optical microscopy images of WEC from a) MTH A 1 test and b) MTH A 7 test. The cuts are in the transverse direction.

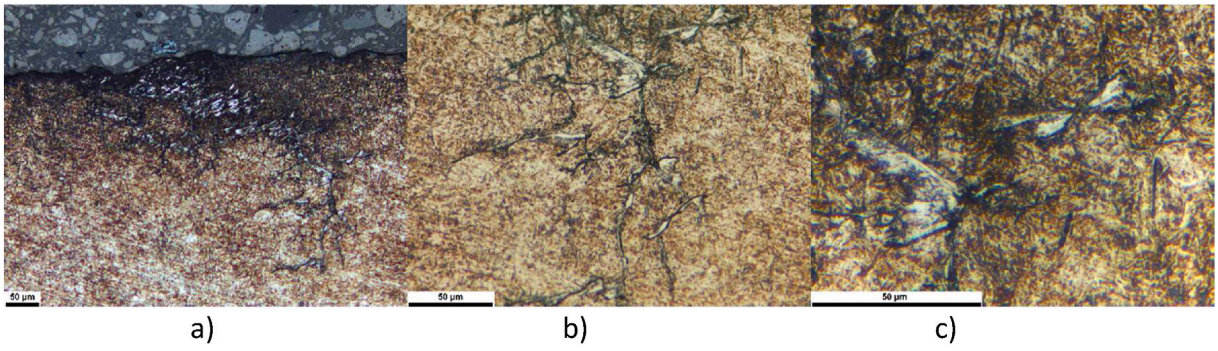

Fig. 8. Optical microscopy of WEC beneath the spall from the CN B 1 test at different magnifications. The cut is along the rolling direction and was the only location where WEC was identified for the CN B material.

reconstructed volumes were filtered by a standard median filter to remove noise. Particle segmentation was then performed by applying a top-hat transform using a ball shaped kernel size 20 for selecting the width of local valleys. The number of local valleys were plotted as a function of local valley depth in grey levels, see Fig. 10a. Based on where the shape of the curves starts deviating from the ideal polynomial noise curve, a cut-off value of 50,000 was chosen for all scans to make them comparable. This corresponds to everything below the grey levels of 2,690, 2,562 and 2,370 respectively for the three scans to be discarded as noise. The choice of remaining grey levels selects the depth of the valleys to be used for segmenting the particles within the analyzed volumes.

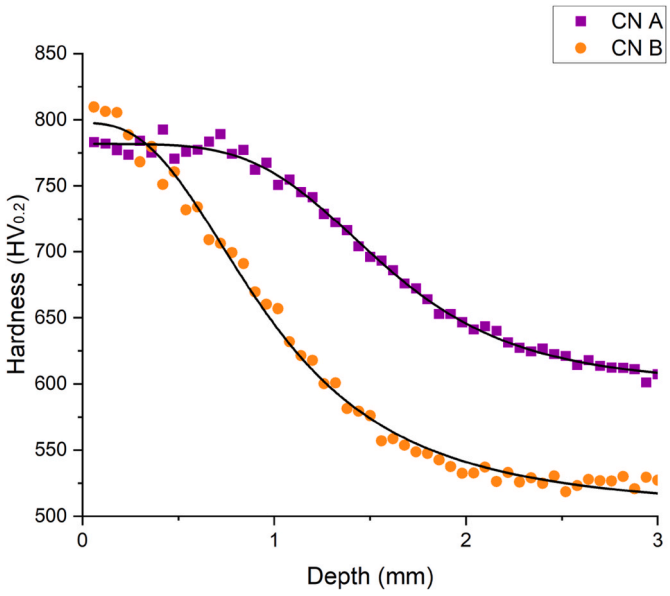

Fig. 9. Hardness profiles for CN A and CN B washers tested during this work.

The segmented volumes were then analyzed to determine the size distribution of the particles/noise, which are illustrated in a semi logarithmic plot in Fig. 10b for the three scans. The number of particles decrease exponentially when the particles size increase from 1 up to 10 voxels, as the first 10 points can be plotted linearly. This indicates particles up to 10 voxels large to be almost exclusively noise. As random noise would be expected to still decrease exponentially with size, the straight line has been extrapolated to indicate the noise level. As the data starts deviating from this straight line, it indicates an increasing ratio of inclusions to noise. Assuming a spherical shape, for particle diameters of ≈3 μm (23 voxels) the signal would consist predominantly of inclusions for all scans, and for particle diameters of ≈3.5 μm (37 voxels) the noise would be negligible for all scans. For this work, a particle size of 37 voxels was applied as the cut-off point for analyzing inclusions to avoid any background noise.

3D reconstructions of the scanned volumes are shown in Fig. 11, with inclusions shown in blue and the steel matrix as transparent. The inclusions in the MTH A and MTH B materials have a similar appearance, with the presence of many large elongated inclusions, presumably MnS. The MTH C material contains a very different population of inclusions, with an almost complete lack of large elongated inclusions that are so prominent for MTH A and MTH B. The number and volume of inclusions is given in Table 7, showing the total number of inclusions to be roughly comparable for all of the materials. However, while the total inclusion volume is comparable for MTH A and MTH B, the MTH C total inclusion volume is far lower. SEM images of the three martensitic through hardened steels are given in Fig. 12, however the true morphology of the inclusions cannot be determined by standard 2D microscopy. EDS measurements of the inclusions indicate them to be primarily MnS, occasionally associated with small amounts of Al_2O_3.

4. Discussion

The results for the baseline tests for MTH A and MTH B washers were very consistent, with time to failure being located within a relatively narrow interval for all ten tests. The baseline tests using washers made from MTH A showed high reproducibility (coefficient of correlation of 0.888) and low scattering (Weibull shape parameter $\beta = 9.9$) and resulted in a lifetime at a failure probability of 10 % of 69.8 h. A Weibull analysis of the MTH B washers is not possible due to the low sample size. Ultrasound measurements backed up by optical microscopy indicated all the baseline tests contained significant amounts of WEC in the failed washers, and frequently in the non-failed ones as well. The MTH C washers required about 4–5 times longer test durations for reaching failure by WEC, although the washer are made from nominally equivalent steel grades. X-ray tomography scans of the washers showed a significant difference in the volume of inclusions, with the total inclusions volume for MTH A and MTH B being more than six times that for MTH C. While there is not a large difference between the washers in the total number of inclusions, the MTH C material essentially contains very few large inclusions above 1000 μm^3. Correlations between WEC and inclusions have previously been reported in Refs. [49–52]. Thus, an explanation for the substantial increase in WEC lifetime of MTH C compared to other standard bearing steels using the accelerated WEC

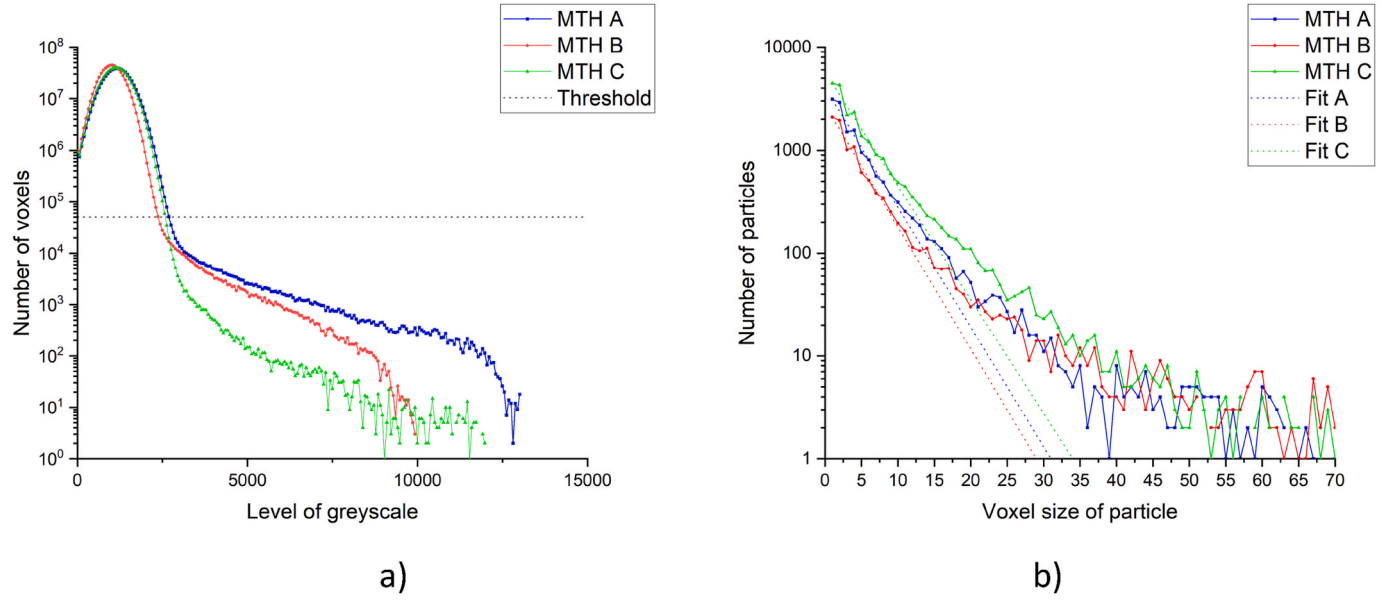

Fig. 10. a) Semi-logarithmic plot for the top-hat transformation of the three X-ray tomography scans. The x-axis shows the grey-level deviation from the background and y-axis the number of voxels with this interval of grey-level deviation. b) Semi-logarithmic plots for the three scans, showing the number of segmented particles as function of the particle size in voxels. The dashed linear fits are based on the first 10 voxel size points.

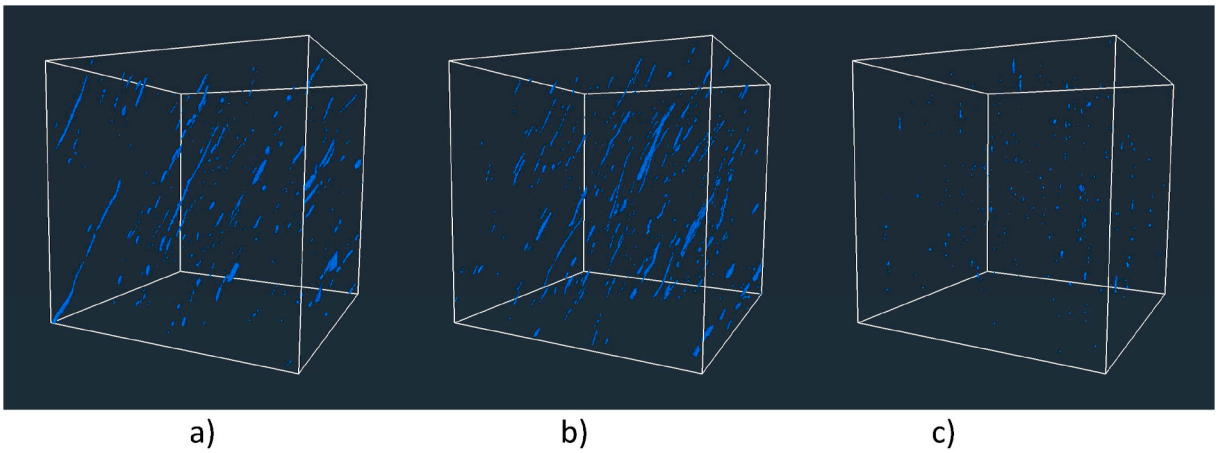

Fig. 11. 3D representation of the for the three X-ray tomography scans, showing the scanned 720 × 720 × 720 μm volumes. Inclusions are displayed in blue and steel matrix as transparent. The volumes are taken from the center of the washer rings to avoid the influence of over rolling, the raceway surface direction is upwards. a) MTH A, b) MTH B and c) MTH C. (For interpretation of the references to colour in this figure legend, the reader is referred to the Web version of this article.)

Table 7
Number and volume of the inclusions within the scanned volume of the martensitic through hardened steels, based on X-ray tomography.

Washer material	Number of inclusions	Volume of inclusion (μm^3)
MTH A	348	214,858
MTH B	451	218,968
MTH C	281	34,293

test setup used in this work, could be the absence of large inclusions. However, other work using FE8 accelerated WEC tests has indicated that the inclusion rating for bearing steels does not influence time to failure [42].

In order to evaluate the effect of roughness on WEC in the FE8 tests, MTH C washers with $R_a = 0.08$ μm and $R_a = 0.03$ μm were tested with resulting specific film thicknesses of 0.47 and 0.77 at 500 rpm, 100 °C and 60 kN, which is within the boundary lubrication regime. Although there was a difference of around 20 % in time to failure, overall the tests showed a similar behavior with WEC failure within the interval of 300–400 h. Thus, the results for MTH C tests would indicate that the different tests done using different washer roughness in this work are comparable. This is in contrast to Ref. [15] that indicates roughness plays an important role for WEC, with smoother bearing components significantly increasing time to failure for FE8 WEC tests (up to 8x). It should be remarked, that for the tests in Ref. [15] both the steel roller and washer roughness were altered, while in this work only the washer roughness was altered while the rolling elements were similar for all of the test. The use of ceramic rollers in this work might also have an effect on the role of washer roughness.

The test performed using standard commercial washers coated with a black oxide layer had a time to failure comparable to the baseline tests. During visual inspection after the test, it was clear that the layer had been completely worn off during the test, thus it would be unable to provide protection against WEC in this test setup. Due to the high share of solid body contact during the tests ($\lambda_{min} < 1$) and the geometrical sliding from the thrust bearings, it can be assumed that the selected conditions might effectively lead to an accelerated wear of the black oxide coating. Once the coating has been removed the risk of WEC formation in MTH A BO washers is similar to the risk in uncoated washers. If the WEC resistance or life time prolongation of black oxide coatings are to be tested, it needs to be done under conditions with lower wear, or at least such that the layer can function properly for the duration of the test.

Overall, the failure mechanism of the CN A surface engineered material was similar to the baseline washers, with clear indications of WEC from both ultrasound measurement and optical microscopy. The tests showed a 4–5 times longer time to failure compared to the baseline tests of MTH A and MTH B, indicating a significant WEC resistance. However, the tests showed no marked improvement compared to MTH C, the averaged time to failures where in fact quite comparable. A Weibull analysis of the MTH C, CN A and CN B washers is not possible due to the low sample size. The washers from the two CN B tests were the only

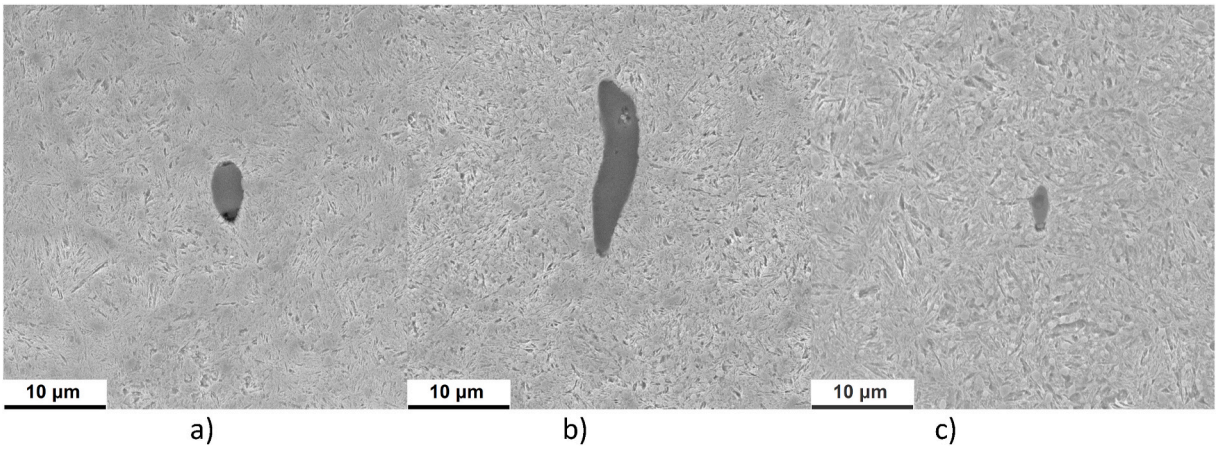

Fig. 12. SEM imaging of MnS inclusions containing small amounts of Al_2O_3 for the martensitic through hardened steels. a) MTH A, b) MTH B and c) MTH C.

washers which did not show any sign of WEC presence in the ultrasound scans, all other tested washers had very clear indications of WEC, at least in the failed washers and in most cases also in the non-failed washers. Thus, the results indicate that CN B material is resistant to WEC formation, with one test even running to time-out (>1400 h). The second test, however, failed due to spalling. The root cause of the failure could have originated in either the steel washer or the failed ceramic roller, with the follow-up damage spreading until the vibration threshold was reached. The test could be considered as a premature failure as no WEC indications were found by ultrasound measurements. However, some local WEC formations were found by optical microscopy beneath the spall of the failed washer, thus demonstrating that the material is not immune to WEC formation. The WEC formation did not appear to have developed as larger crack networks as observed in other tested materials, although the most severe WEC areas might have spalled off. As no other WEC affect areas could be identified by ultrasound or microscopy it is difficult to estimate if the failure was indeed caused by WEC or due to other failure mechanisms such as classic fatigue.

5. Conclusion

During this work an accelerated WEC test setup with FE8 type test rigs and ceramic rollers was used for determining the WEC lifetime of different washer bearing materials, materials quality and roughness. The WEC resistance of the commercially available bearing materials can be summed up as follows:

- It was demonstrated that accelerated WEC tests in FE8 type test rigs using ceramic rollers can reliably be carried out on commercially bought washers with a very consistent time to failure from WEC, confirmed through ultrasound measurements and optical microscopy.
- Standard through hardened bearing steel washers with very low content of large inclusions consistently had significantly longer time to failure compared to other standard through hardened bearing steels with a similar number of inclusions. This might indicate the absence of large inclusions affects the WEC formation.
- Unexpectedly, lowering the roughness of comparable washers did not result in a higher time to failure. Further investigations may be needed in order to assess the role of the surface roughness on the WEC formation.
- Commercial washers coated with black oxide did not provide any WEC resistance, the time to failure was in line with un-coated washers. The black oxide coating was worn away in the contact zone during the test, indicating the test setup is not suitable for evaluating the WEC resistance of black oxide coatings.
- One of the two types of tested carbo-nitrided washers showed high resistance to WEC, to a degree where WEC could not be detected using ultrasound measurements after prolonged test duration. However, local WEC formation was found using optical microscopy, demonstrating the material is not immune to WEC formation. The second type of tested carbo-nitrided washers showed a similar performance to the standard through hardened bearing steel washers with reduced volume of inclusions.

CRediT authorship contribution statement

H.K. Danielsen: Conceptualization, Methodology, Resources, Formal analysis, Writing – original draft, Supervision, Project administration, Funding acquisition. **F. Gutiérrez Guzmán:** Formal analysis, Writing – review & editing. **S. Fæster:** Investigation, Formal analysis, Visualization, Writing – review & editing. **M. Shirani:** Investigation. **B. H. Rasmussen:** Investigation. **M. Linzmayer:** Formal analysis. **G. Jacobs:** Writing – review & editing.

Declaration of competing interest

The authors declare that they have no known competing financial interests or personal relationships that could have appeared to influence the work reported in this paper.

Acknowledgements

This project was sponsored by the Innovation Fund Denmark grant number 7046-00003B. NSK Deutschland GmbH is thanked for providing washers for testing.

Appendix A. Supplementary data

Supplementary data to this article can be found online at https://doi.org/10.1016/j.wear.2021.204230.

References

[1] B. Gould, N.G. Demas, A.C. Greco, The Influence of steel Microstructure and inclusion Characteristics on the Formation of premature bearing Failures with microstructural alterations, Mater. Sci. Eng., A 751 (2019) 237–245, https://doi.org/10.1016/j.msea.2019.02.084.
[2] M.H. Evans, An updated review: white etching cracks (WECs) and axial cracks in wind turbine gearbox bearings, Mater. Sci. Technol. 32 (2016) 1133–1169, https://doi.org/10.1080/02670836.2015.1133022.
[3] K. Stadler, J. Lai, R.H. Vegter, *A Review: the Dilemma with Premature White Etching Crack (WEC) Bearing Failures* Bearing Steel Technologies: 10th Volume, Advances in Steel Technologies for Rolling Bearings STP 1580, 2014.
[4] J. Luyckx, White etching crack failure mode in roller bearings: from observation via analysis to understanding and an industrial solution, Rolling Elements Bearings 9 (2012) 1–25, https://doi.org/10.1520/STP103908.
[5] A. Grabulov, R. Petrov, H.W. Zandbergen, EBSD investigation of the crack initiation and TEM/FIB analyses of the microstructural changes around the cracks formed under Rolling Contact Fatigue (RCF), Int. J. Fatig. 32 (2010) 576–583, https://doi.org/10.1016/j.ijfatigue.2009.07.002.
[6] M.H. Evans, J.C. Walker, C. Ma, L. Wang, R.J.K. Wood, A FIB/TEM study of butter fly crack formation and white etching area (WEA) microstructural changes under rolling contact fatigue in 100Cr6 bearing steel, Mater. Sci. Eng., A 570 (2013) 127–134, https://doi.org/10.1016/j.msea.2013.02.004.
[7] H.K. Danielsen, F. Gutiérrez Guzmán, K.V. Dahl, Y.J. Li, J. Wu, G. Jacobs, G. Burghardt, S. Fæster, H. Alimadadi, S. Goto, D. Raabe, R. Petrov, Multiscale characterization of White Etching Cracks (WEC) in a 100Cr6 bearing from a thrust bearing test rig, Wear 370–371 (2017) 73–82, https://doi.org/10.1016/j.wear.2016.11.016.
[8] M.E. Curd, T.L. Burnett, J. Fellowes, J. Yan, P.J. Withers, Redistribution of carbon caused by butterfly defects in bearing steels, Acta Mater. 183 (2020) 390–397.
[9] Y.J. Li, M. Herbig, S. Goto, D. Raabe, Atomic scale characterization of white etching area and its adjacent matrix in a martensitic 100Cr6 bearing steel, Mater. Char. 123 (2017) 349–353.
[10] D. Mayweg, L. Morsdorf, X. Wu, M. Herbig, The role of carbon in the white etching crack phenomenon in bearing steels, Acta Mater. 203 (2021), 116480.
[11] V. Šmeļova, A. Schwedt, L. Wang, W. Holweger, J. Mayer, Microstructural changes in white etching cracks (WECs) and their relationship with those in dark etching region (DER) and white etching bands (WEBs) due to rolling contact fatigue (RCF), Int. J. Fatig. 100 (2017) 148–158.
[12] D. Mayweg, L. Morsdorf, Y. Li, M. Herbig, Correlation between grain size and carbon content in white etching areas in bearings, Acta Mater. 215 (2021), 117048.
[13] H.K. Danielsen, C. Hong, O.V. Mishin, Microstructural characterization of white etching cracks in bearings after long-term operation in wind turbines, Mater. Lett. 294 (2021), 129754.
[14] W. Holweger, M. Wolf, D. Merk, T. Blass, M. Goss, J. Loos, S. Barteldes, A. Jakovics, White etching crack root cause investigations, Tribol. Trans. 58 (2015) 59–69, https://doi.org/10.1080/10402004.2014.942938.
[15] W. Kruhöffer, J. Loos, WEC Formation in rolling Bearings under mixed friction: Influences and "friction energy accumulation" as indicator, Tribol. Trans. 60 (2017) 516–529, https://doi.org/10.1080/10402004.2016.1183250.
[16] A. Ruellan, X. Kleber, F. Ville, J. Cavoret, B. Liatard, Understanding white etching cracks in rolling element bearings: Formation mechanisms and influent tribochemical drivers, Proc IMechE Part J: J. Eng. Tribol. 229 (2015) 886–901, https://doi.org/10.1177/1350650114557710.
[17] M.H. Evans, A.D. Richardson, L. Wang, R.J.K. Wood, W.B. Anderson, Confirming subsurface initiation at non-metallic inclusions as one mechanism for white etching crack (WEC) formation, Tribol. Int. 75 (2014) 87–97, https://doi.org/10.1016/j.triboint.2014.03.012.
[18] M. Oezel, A. Schwedt, T. Janitzky, R. Kelley, C. Bouchet-Marquis, L. Pullan, C. Broeckmann, J. Mayer, Formation of white etching areas in SAE 52100 bearing steel under rolling contact fatigue - influence of diffusible hydrogen, Wear 414–415 (2018) 352–365.

[19] M.E. Curd, T.L. Burnett, J. Fellowes, J. Donoghue, P. Yan, P.J. Withers, The heterogenous distribution of white etching matter (WEM) around subsurface cracks in bearing steels, Acta Mater. 174 (2019) 300–309.

[20] F. Manieri, K. Stadler, G.E. Morales-Espejel, A. Kadirica, The origins of white etching cracks and their significance to rolling bearing failures, Int. J. Fatig. 120 (2019) 107–133, https://doi.org/10.1016/j.ijfatigue.2018.10.023.

[21] L. Morsdorf, D. Mayweg, Y. Li, A. Diederichs, D. Raabe, M. Herbig, Moving cracks form white etching areas during rolling contact fatigue in bearings, Mater. Sci. Eng. 771 (2020), 138659.

[22] B. Gould, M. Paladugu, N.G. Demas, A.C. Greco, R.S. Hyde, Figure the impact of steel microstructure and heat treatment on the formation of white etching cracks, Tribol. Int. 134 (2019) 232–239, https://doi.org/10.1016/j.triboint.2019.02.003.

[23] H.A. Al-Tameemi, H. Long, R.S. Dwyer-Joyce, Damage characterisation of white etching cracks in a black oxide coated wind turbine gearbox bearing, Wear 432–433 (2019), 102923, https://doi.org/10.1016/j.wear.2019.05.038.

[24] T. Blass, W. Trojahn, D. Merk, *Influence Of Material And Heat Treatment On the Formation Of WECs On Test Rig FE8* STP 1600, 2017, https://doi.org/10.1520/STP160020160139.

[25] A. Greco, S. Sheng, J. Keller, A. Erdemir, Material wear and fatigue in wind turbine Systems, Wear 302 (2013) 1583–1591, https://doi.org/10.1016/j.wear.2013.01.060.

[26] R.H. Vegter, J.T. Slycke, J. Beswick, S.W. Dean, The role of hydrogen on rolling contact fatigue response of rolling element bearings, J. ASTM Int. (JAI) 7 (2009), 102543.

[27] H. Uyama, H. Yamada, H. Hidaka, N. Mitamura, The effect on hydrogen on microstructure change and surface originated flaking in rolling contact fatigue, Tribol. Online 6 (2011) 123–132, https://doi.org/10.2474/troll.6.123.

[28] M.H. Evans, A.D. Richardson, L. Wang, R.J.K. Wood, Effect of hydrogen on butterfly and white etching crack (WEC) formation under rolling contact fatigue (RCF), Wear 306 (2013) 226–241, https://doi.org/10.1016/j.wear.2013.03.008.

[29] T. Haque, S. Korres, J.T. Carey, P.W. Jacobs, J. Loos, J. Franke, Lubricant effects on white etching cracking failures in thrust bearing rig tests, Tribol. Trans. 61 (2018) 979–990, https://doi.org/10.1080/10402004.2018.1453571.

[30] M. Paladugu, D.R. Lucas, R.S. Hyde, Effect of lubricants on bearing damage in rolling-sliding conditions: Evolution of white etching cracks, Wear 398–399 (2018) 165–177, https://doi.org/10.1016/j.wear.2017.12.001.

[31] B. Gould, N.G. Demas, G. Pollard, J.J. Rydel, M. Ingram, A.C. Greco, The effect of lubricant composition on white etching crack failures, Tribol. Lett. 67 (2019) 7, https://doi.org/10.1007/s11249-018-1106-y.

[32] B. Gould, A. Greco, The influence of sliding and contact severity on the generation of white etching cracks, Tribol. Lett. 60 (2015) 29, https://doi.org/10.1007/s11249-015-0602-6.

[33] B. Gould, A. Greco, Investigating the process of white etching crack initiation in bearing steel, Tribol. Lett. 62 (2016) 26, https://doi.org/10.1007/s11249-016-0673-z.

[34] F.G. Guzmán, M.O. Oezel, G. Jacobs, G. Burghardt, C. Broeckmann, T. Janitzky, Influence of slip and lubrication regime on the formation of white etching cracks on a two-disc test rig, Lubricants 6 (2018), https://doi.org/10.3390/lubricants6010008.

[35] J. Loos, I. Bergmann, M. Goss, Influence of Currents from electrostatic Charges on WEC Formation in rolling bearings, Tribol. Trans. 59 (2016) 865–875, https://doi.org/10.1080/10402004.2015.1118582.

[36] M. Hidenobu, K. Takayuki, Influence Of Electrical Current on Bearing Flaking Life, SAE International, 2007, https://doi.org/10.4271/2007-01-0113. World Congress.

[37] A.M. Diederichs, S. Barteldes, A. Schwedt, J. Mayer, W. Holweger, Study of subsurface initiation mechanism for white etching crack formation, Mater. Sci. Technol. 32 (2016) 1170–1178, https://doi.org/10.1080/02670836.2016.1155842.

[38] A.D. Richardson, M.H. Evans, L. Wang, R.J.K. Wood, M. Ingram, B. Meuth, The evolution of white etching cracks (WECs) in rolling contact fatigue-tested 100Cr6 steel, Tribol. Lett. 66 (2018), https://doi.org/10.1007/s11249-017-0946-1.

[39] F. Gutiérrez Guzmán, M. Oezel, G. Jacobs, G. Burghardt, C. Broeckmann, T. Janitzky, Reproduction of white etching cracks under rolling contact loading on thrust bearing and two-disc test rigs, Wear 390–391 (2017) 23–32, https://doi.org/10.1016/j.wear.2017.06.020.

[40] H.K. Danielsen, A.J. Carrasco, S. Fæster, K.V. Dahl, F. Gutiérrez Guzmán, P. Sauvage, G. Jacobs, 3D X-ray computerized tomography of white etching cracks (WEC), Mater. Char. 150 (2019) 78–87, https://doi.org/10.1016/j.matchar.2019.01.032.

[41] H.K. Danielsen, F. Gutierrez Guzmán, M. Muskulus, B.H. Rasmussen, M. Shirani, D. Cornel, P. Sauvage, J. Wu, R. Petrov, G. Jacobs, FE8 type laboratory testing of white etching crack (WEC) bearing failure mode in 100Cr6, Wear 434–435 (2019), 202962, https://doi.org/10.1016/j.wear.2019.202962.

[42] J. Loos, T. Blass, J. Franke, W. Kruhoeffer, I. Bergmann, Influences on generation of white etching crack networks in rolling bearings, J. Mech. Eng. Autom. 6 (2016) 85–94, https://doi.org/10.17265/2159-5275/2016.02.004.

[43] D. Dowson, G.R. Higginson, Elasto-Hydrodynamic Lubrication, Pergamon Press, Oxford, 1977.

[44] DIN EN 61649 Weibull-Analyse (2008) (IEC 61649 2008-08).

[45] M. Linzmayer, C. Sous, F. Gutiérrez Guzmán, G. Jacobs, Interlaboratory comparison: round robin test for the damage reproduction of white etching crack in cylindrical roller thrust bearings, Wear 480–481 (2021), 203925, https://doi.org/10.1016/j.wear.2021.203925.

[46] e.V. Deutsches Institut für Normung, DIN ISO 281, Wälzlager - Dynamische Tragzahlen und nominelle Lebensdauer, 2010.

[47] B.L. Vlcek, C. Hendricks, E.V. Zaretsky, Monte Carlo simulation of sudden death bearing testing, Tribol. Trans. 47 (2004) 188–199, https://doi.org/10.1080/05698190490431867.

[48] K. Stadler, E. Vegter, M. Ersson, D. Vaes, in: White Etching Cracks - a Symptom of Bearing Failures FVA Bearing World Conference, 2016, pp. 245–263.

[49] M.W.J. Lewis, N. Tomkins, *A fracture mechanics interpretation of rolling bearing fatigue* Proceedings of the Institution of Mechanical Engineers, Part J: J. Eng. Tribol. 226 (2012) 389–405.

[50] M.H. Evans, L. Wang, H. Jones, R.J.K. Wood, White etching crack (WEC) investigation by serial sectioning, focused ion beam and 3-D crack modelling, Tribol. Int. 65 (2013) 146–160.

[51] H.A. Al-Tameemi, H. Long, R.S. Dwyer-Joyce, Initiation of sub-surface micro-cracks and white etching areas from debonding at non-metallic inclusions in wind turbine gearbox bearing, Wear 406–407 (2018) 22–32.

[52] B. Gould, A. Greco, K. Stadler, E. Vegter, X. Xiao, Using advanced tomography techniques to investigate the development of White Etching Cracks in a prematurely failed field bearing, Tribol. Int. 116 (2017) 362–370.